Electronic Supporting Information (ESI)

Multi-channel photodissociation and XUV-induced charge transfer dynamics in strong-field-ionized methyl iodide studied with time-resolved recoil-frame covariance imaging

October 5, 2020

Felix Allum,[a] Nils Anders,[b] Mark Brouard,[a] Philip Bucksbaum,[c] Michael Burt,[a] Briony Downes-Ward,[d] Sven Grundmann,[b] James Harries,[e] Yudai Ishimura,[f] Hiroshi Iwayama,[g] Leon Kaiser,[b] Edwin Kukk,[h] Jason Lee,[i] Xiaojing Liu,[j] Russell S. Minns,[d] Kiyonobu Nagaya,[k] Akinobu Niozu,[k] Johannes Niskanen,[h] Jordan O'Neal,[c] Shigeki Owada,[l] James Pickering,[a] Daniel Rolles,[m] Artem Rudenko,[m] Shu Saito,[f] Kiyoshi Ueda,[f] Claire Vallance,[a] Nicholas Werby,[c] Joanne Woodhouse,[d] Daehyun You,[f] Farzaneh Ziaee,[m] Taran Driver,[c] and Ruaridh Forbes[c]

Notes and references

[1] M. E. Corrales, G. Gitzinger, J. González-Vázquez, V. Loriot, R. de Nalda and L. Bañares, *J. Phys. Chem. A*, 2012, **116**, 2669–2677.

[a] *Chemistry Research Laboratory, Department of Chemistry, University of Oxford, Oxford OX1 3TA, United Kingdom*
[b] *Institut für Kernphysik, Goethe-Universität, Max-von-Laue-Strasse 1, 60438 Frankfurt am Main, Germany*
[c] *Stanford PULSE Institute, SLAC National Accelerator Laboratory, 2575 Sand Hill Road, Menlo Park, CA 94025*
[d] *Chemistry, University of Southampton, Highfield, Southampton SO17 1BJ, UK*
[e] *QST, SPring-8, Kouto 1-1-1, Sayo, Hyogo, 679-5148, Japan*
[f] *Institute of Multidisciplinary Research for Advanced Materials, Tohoku University, Sendai, 980-8577, Japan*
[g] *UVSOR Synchrotron Facility, Institute for Molecular Science, Okazaki 444-8585, Japan*
[h] *Department of Physics and Astronomy, University of Turku, Turku, FI-20014, Finland*
[i] *Deutsches Elektronen-Synchrotron (DESY), Notkestraße 85, 22607 Hamburg, Germany*
[j] *School of physical science and technology, ShanghaiTech University, Shanghai, 201210, China*
[k] *Department of Physics, Kyoto University, Kyoto, 606-8502, Japan*
[l] *RIKEN SPring-8 Center, Sayo, Hyogo, 679-5148, Japan*
[m] *J. R. Macdonald Laboratory, Department of Physics, Kansas State University, Manhattan, KS, 66506, USA*

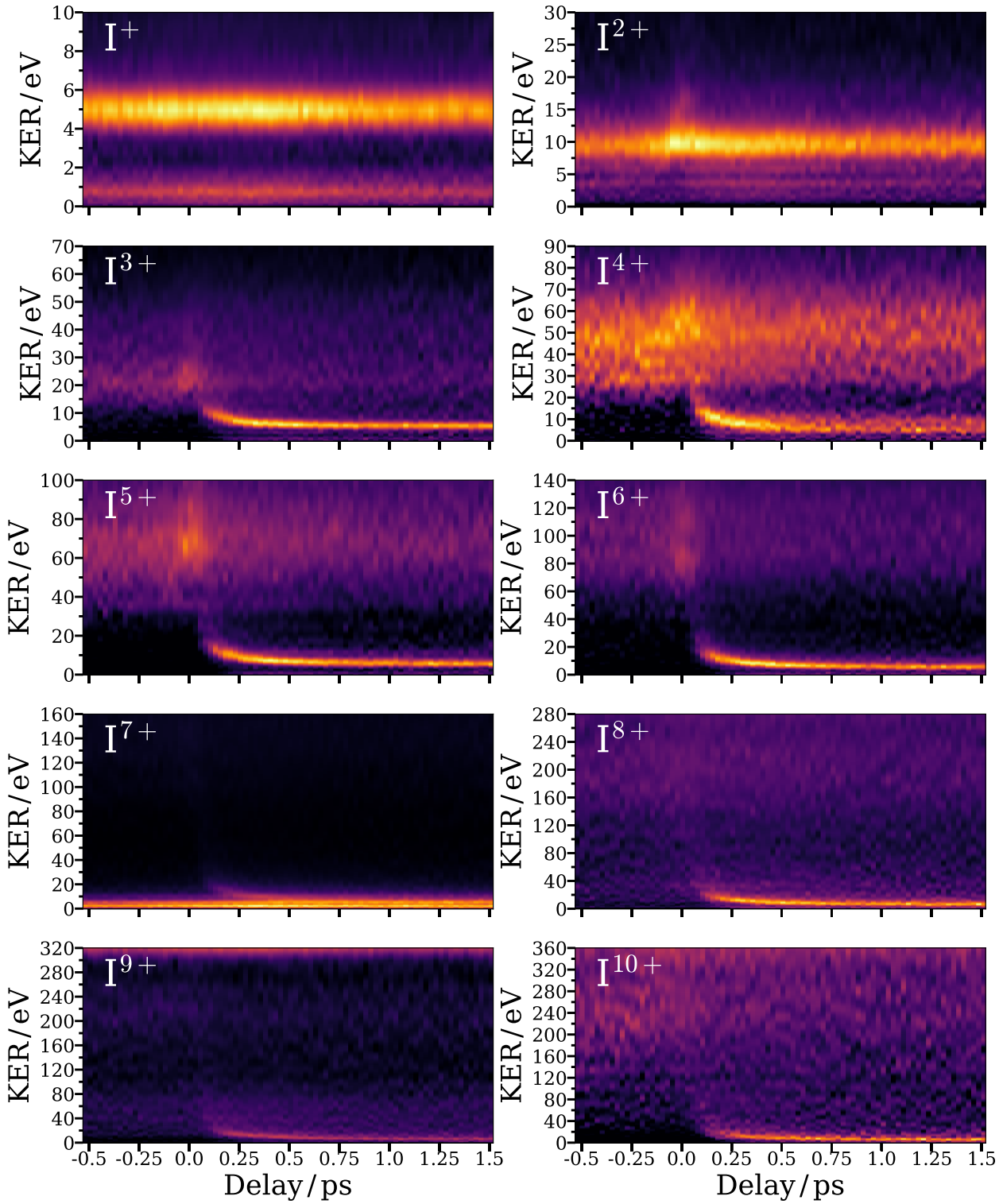

Figure S1 Delay-dependent KER distributions for I^{n+} ions (n=1-10). These are obtained through angular integration of the appropriate time-resolved ion images, following Abel inversion using the pBASEX algorithm. Negative delays correspond to the FEL probe pulse arriving before the IR pump pulse, and vice versa. The $I^{7)}$ ion overlaps in time-of-flight with water, leading to a prominent low KER background. The I^{8+}, I^{9+} and I^{10+} ions overlap in time-of-flight with CH_x^+ ions, leading to some false signal at high KER.

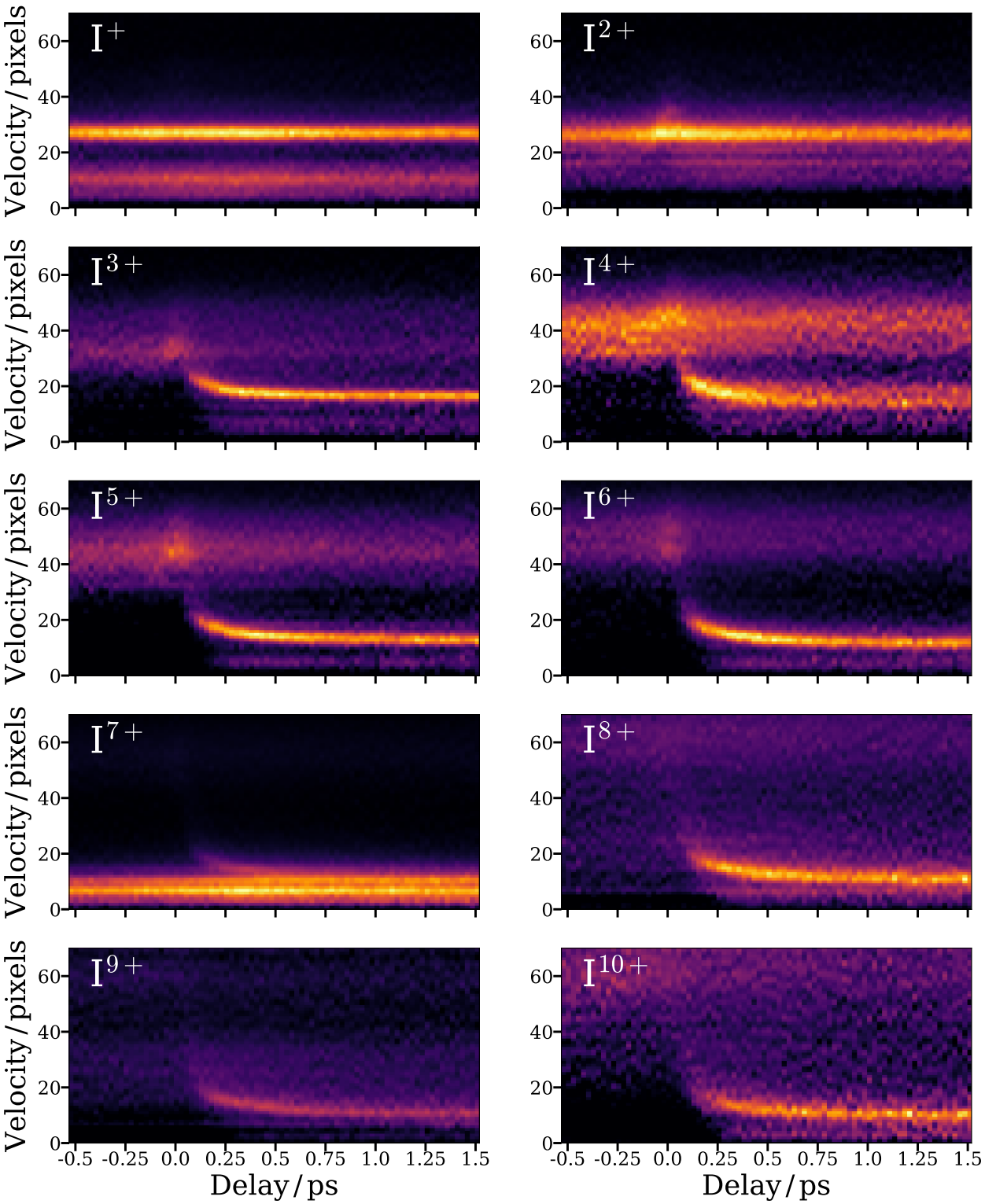

Figure S2 Delay-dependent velocity distributions for I^{n+} ions (n=1-10). These are obtained through angular integration of the appropriate time-resolved ion images, following Abel inversion using the pBASEX algorithm. Intensities are weighted by a factor of 1/velocity in order to enhance visibility of the low velocity features (referred to as Channel III in the main text). Negative delays correspond to the FEL probe pulse arriving before the IR pump pulse, and vice versa. The $I^{7)}$ ion overlaps in time-of-flight with water, leading to a prominent low velocity background. The I^{8+}, I^{9+} and I^{10+} ions overlap in time-of-flight with CH_x^+ ions, leading to some false signal at high velocity.

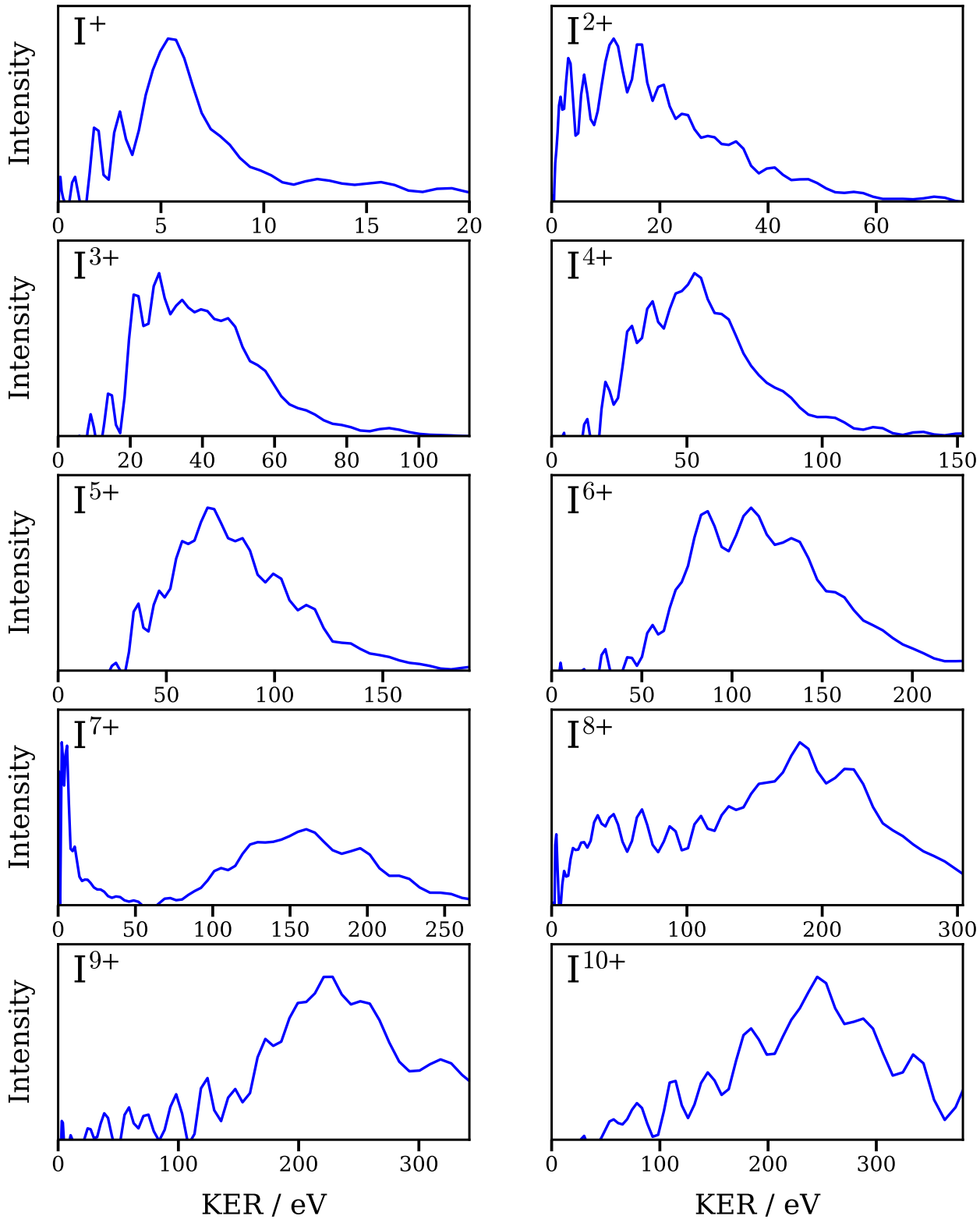

Figure S3 XUV-only KER spectra for I^{n+} ions (n=1-10) ions. These are obtained through angular integration of the appropriate time-resolved ion images, following Abel inversion using the pBASEX algorithm. The $I^{7)}$ ion overlaps in time-of-flight with water, leading to a prominent low KER background. The I^{8+}, I^{9+} and I^{10+} ions overlap in time-of-flight with CH_x^+ ions, leading to some false signal at high KER.

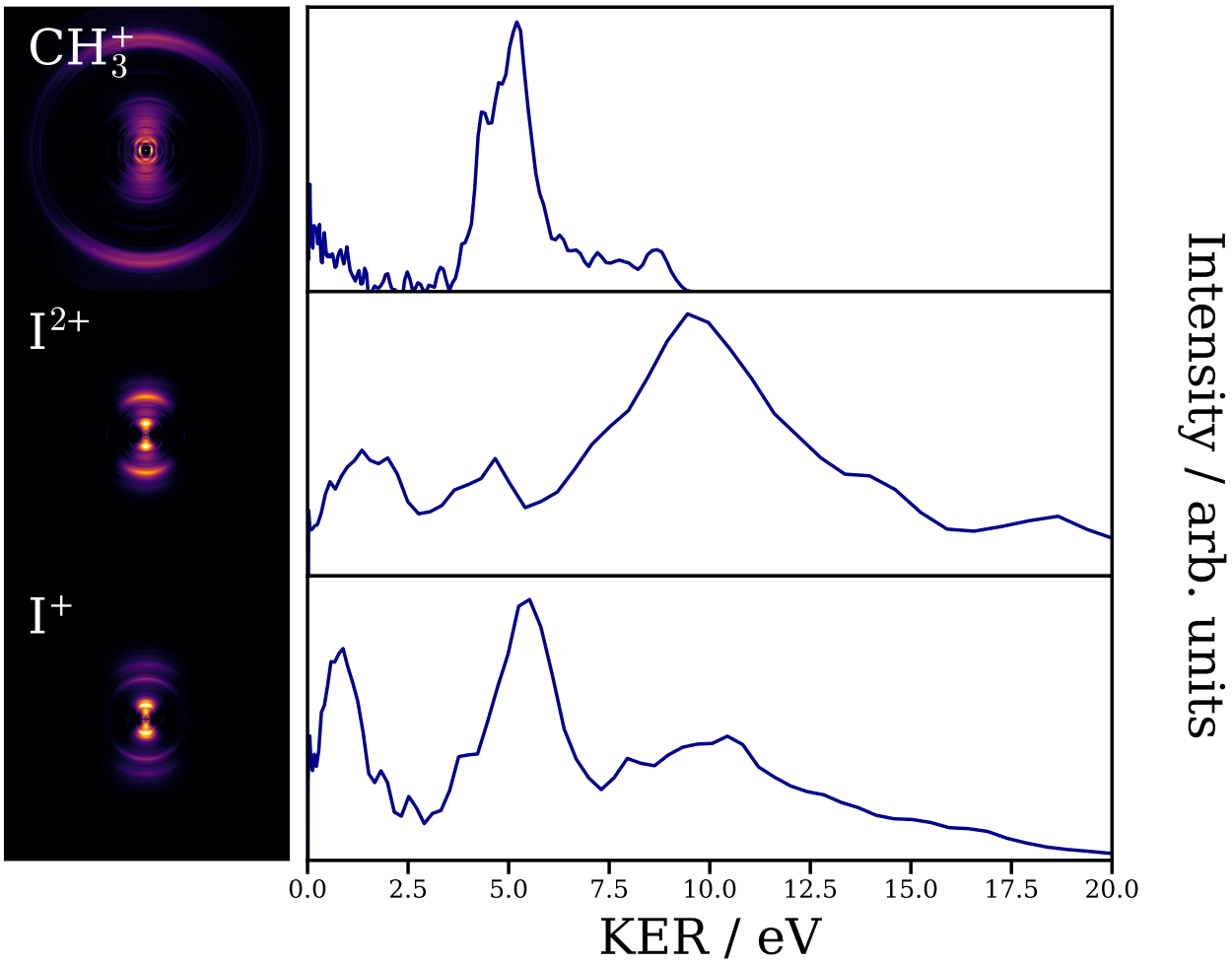

Figure S4 IR-only velocity-map ion images (left) and KER distributions (right) for the CH_3^+, I^{2+} and I^+ ions. These data were recorded with lower spectrometer voltages (half those employed for the data presented in the main text) in order to expand the velocity-map images.

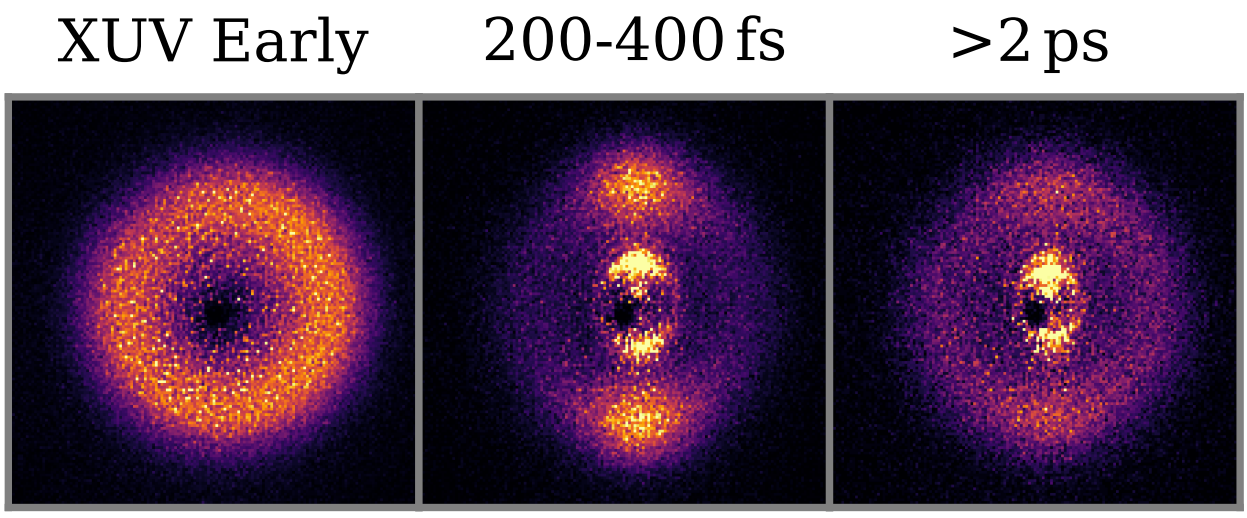

Figure S5 Delay-dependent raw (unprocessed) velocity-map ion images of the I^{5+} ion. These highlight the significant anisotropy in parent Coulomb explosion feature in the 200-400 fs range, arising from impulsive alignment by the IR pulse.

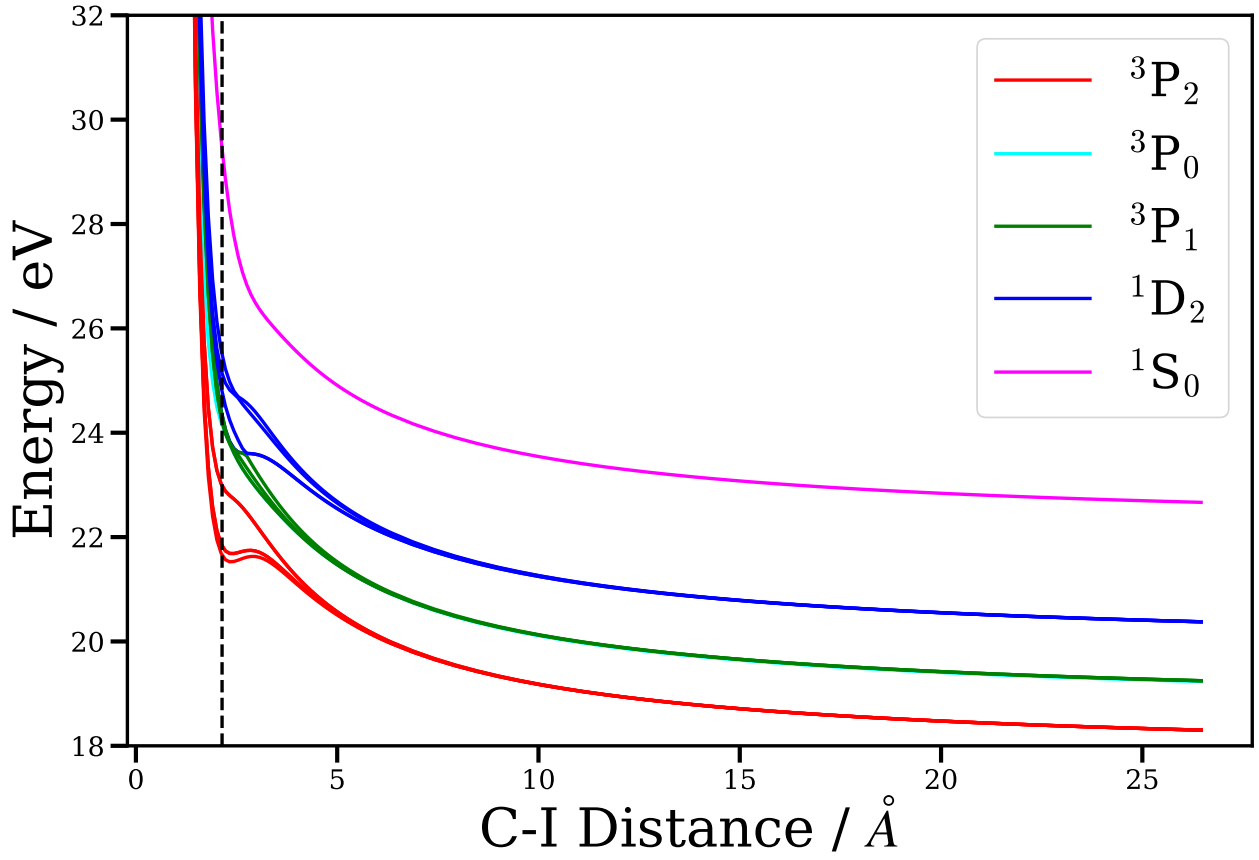

Figure S6 Potential energy curves of the CH_3I^{2+} ion computed by Corrales et. al[1]. Different potentials are labelled by the state of the I^+ cation they correlate with.

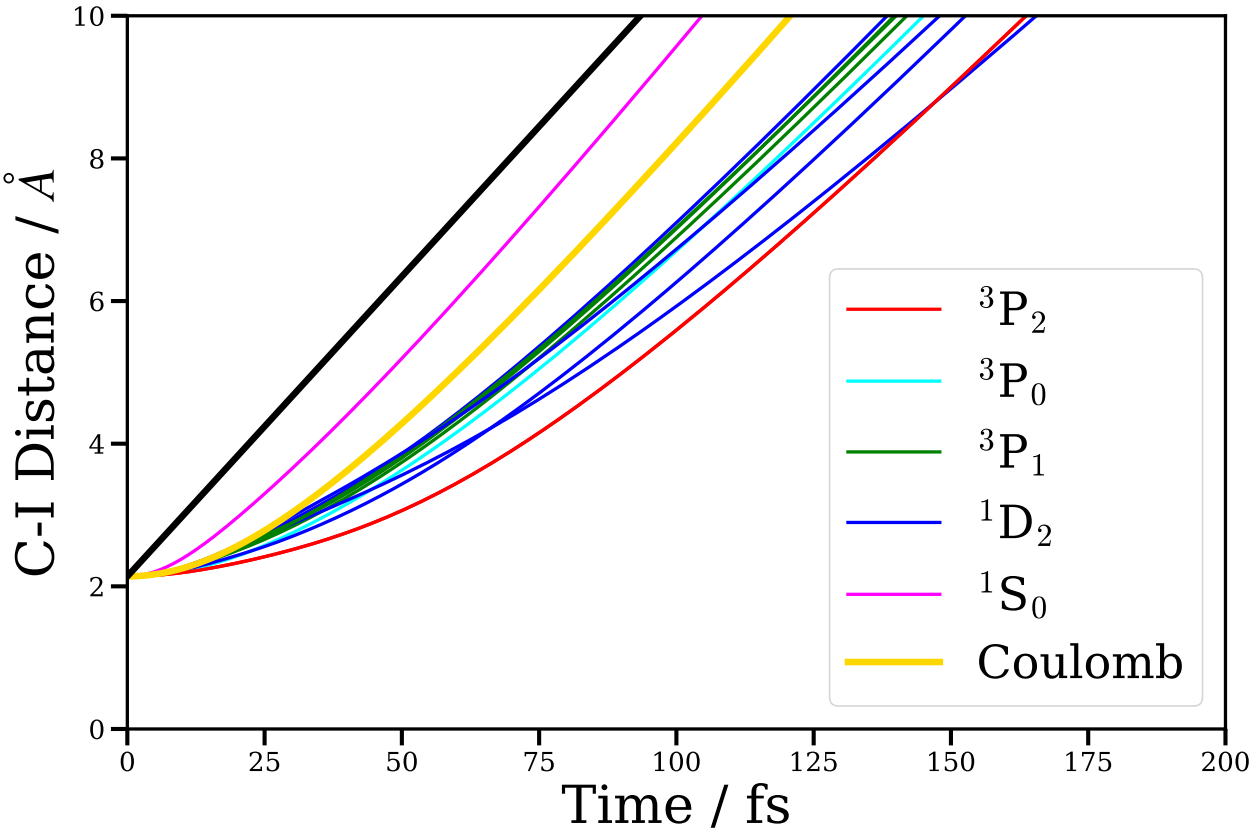

Figure S7 The C-I bond distance as a function of delay for classical trajectory calculations carried out on the computed CH_3I^{2+} potentials, as described in Section 4.2.2 of the main text. States correlating with $^3P_2$ I^+ with bound character are excluded. For comparison, a trajectory assuming instant acceleration to an asymptotic KER of 5.20 eV is shown in black. A trajectory assuming a purely Coulomb (1,1) potential energy surface is also shown in gold.

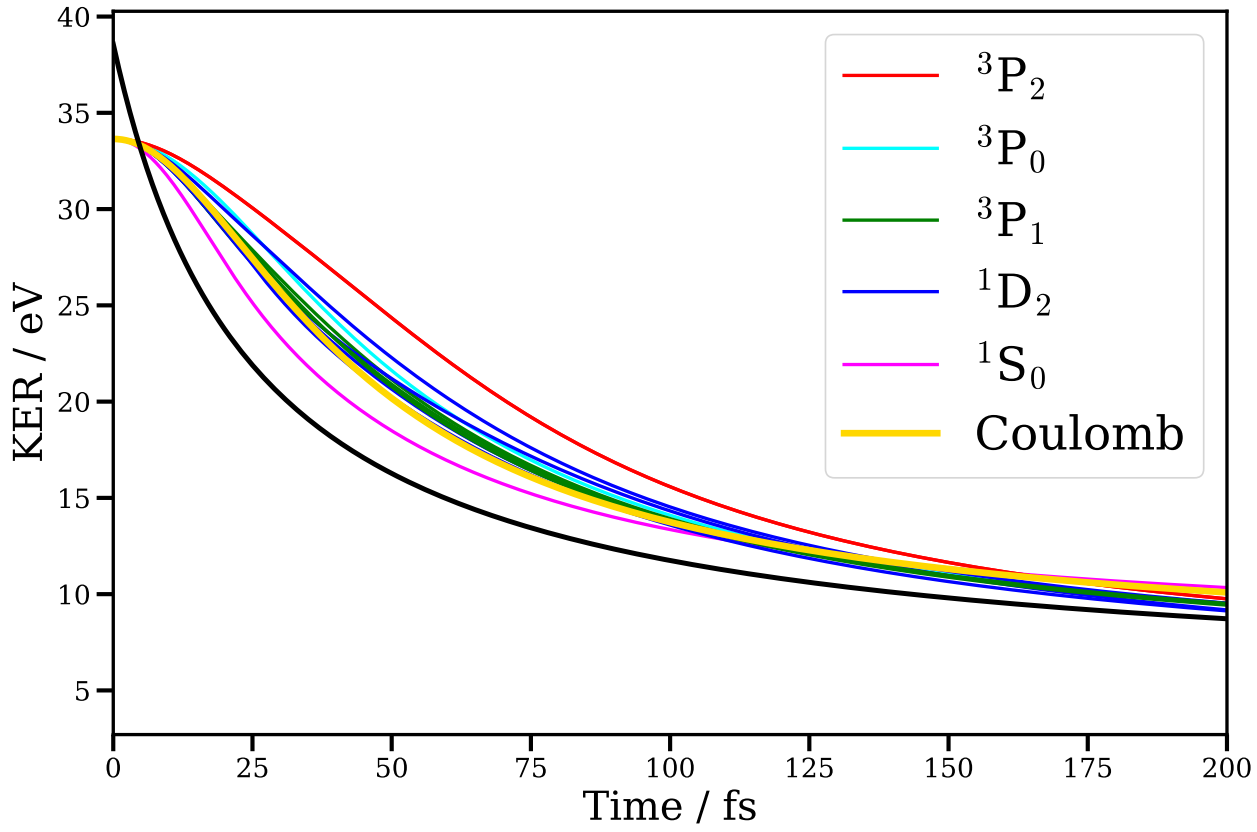

Figure S8 KER as a function of pump-probe delay (0-200 fs range) for the trajectories shown in Figure S7, for XUV ionization of nascent I^+ to I^{5+} as an example, which repel the recoiling CH_3 ion according to Coulomb's Law. Trajectories on the computed CH_3I^{2+} potentials exhibit higher KER in the ~25-200 fs delay range, as discussed in the main text.

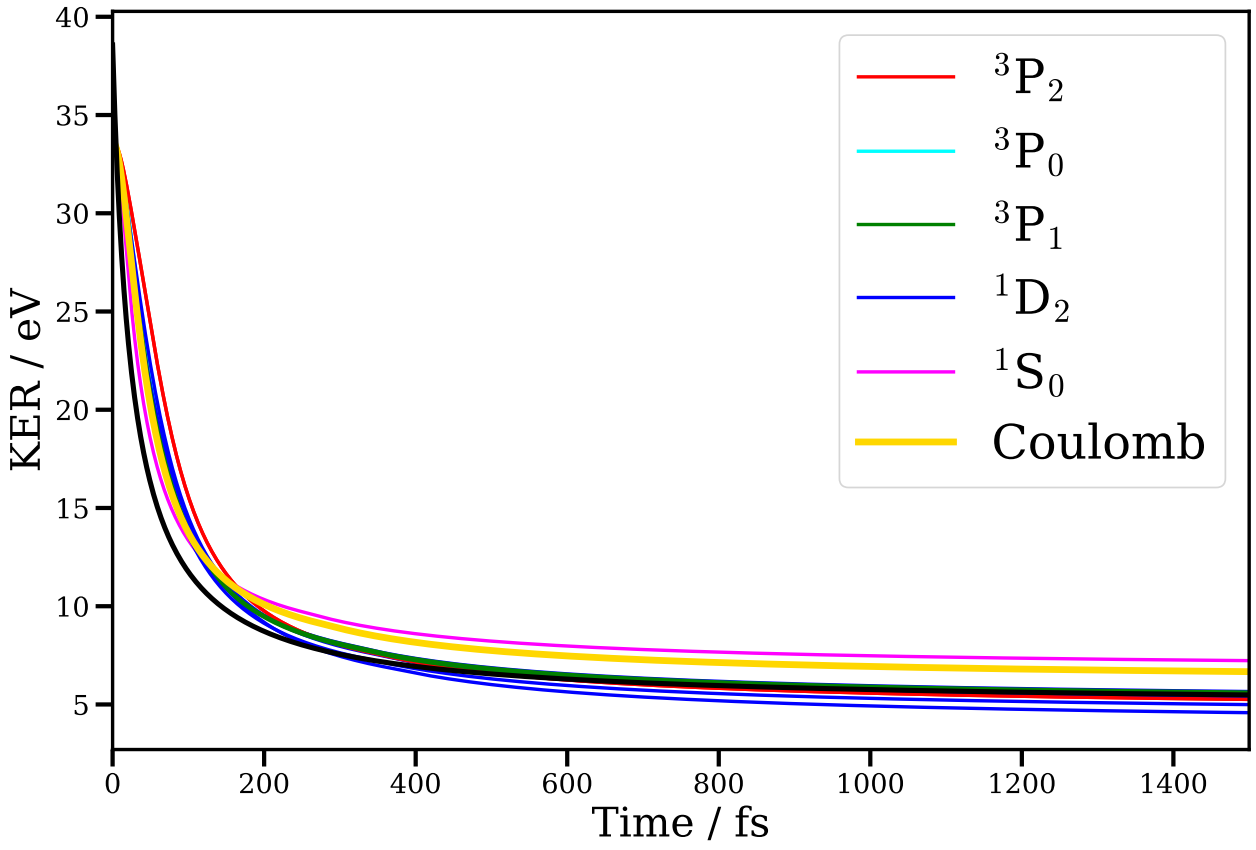

Figure S9 KER as a function of pump-probe delay (0-1500 fs range) for the trajectories shown in Figure S7, for XUV ionization of nascent I^+ to I^{5+}, which repel the recoiling CH_3 ion according to Coulomb's Law.